Ocean Sci. Discuss., 12, 1051–1082, 2015
www.ocean-sci-discuss.net/12/1051/2015/
doi:10.5194/osd-12-1051-2015

Ocean Science
Discussions
Open Access

Discussion Paper | Discussion Paper | Discussion Paper | Discussion Paper |

Estimation of upward radiances and reflectances at the surface of the sea from above-surface measurements

Ø. Kleiv[1], A. Folkestad[1,*], J. Høkedal[2], K. Sørensen[1], and E. Aas[3]

[1]Norwegian Institute for Water Research, Gaustadalleen 21, 0349 Oslo, Norway
[2]Narvik University College, Lodve Langes gt. 2, 8505 Narvik, Norway
[3]Department of Geosciences, University of Oslo, Gaustadalleen 21, 0349 Oslo, Norway
[*]now at: Rolls-Royce Marine Propulsion, Sjøgata 98, 6065 Ulsteinsvik, Norway

Received: 6 May 2015 – Accepted: 19 May 2015 – Published: 12 June 2015

Correspondence to: E. Aas (eyvind.aas@geo.uio.no)

Published by Copernicus Publications on behalf of the European Geosciences Union.

Abstract

During four field days in the years 2009–2011, 22 series of measurement were collected in the Inner Oslofjord. The data consist of recordings of spectral sub-surface and above-surface nadir radiances, as well as spectral downward irradiance in air. The studied wavelengths are 351, 400 nm and the 10 former MERIS channels in the range 413–754 nm.

The water-leaving radiance and the reflected radiance at the sea surface can be determined from the measured nadir radiances in water and air. A simpler and much faster method, which determines the radiance reflectance at the surface as well as the water-leaving and reflected radiances solely from the measurements of upward nadir radiance and downward irradiance in air, is presented.

A comparison between the quantities determined by the two methods shows that the average relative deviations between their results are less than or equal to 15 % for the reflected radiance, at the studied wavelengths. The average relative deviations of the water-leaving radiance at 560 nm is 24 %. We consider this to be acceptable uncertainties for a first check of satellite products in coastal waters.

1 Introduction

The Norwegian Institute for Water Research (NIVA) has been monitoring the coastal waters of Norway by sensors installed onboard ships on fixed and regular routes since 2001, in the FerryBox project and different ESA projects (Sørensen et al., 2007). The need for such monitoring rose during the period 1988–2001 when several toxic algal blooms occured in the Skagerrak and resulted in severe losses for fish farms along the coast (for references see e.g. Kristiansen and Aas, 2015). Monitoring is also an important part of obligations set out in the EU Water Framework Directive. The recordings can be coordinated with data from environmental satellites and used for validation purposes. The projects VAMP (Validation of MERIS Products), supported by the ESA, and REVAMP (Regional Validation of MERIS Products), supported by the EU, are examples of such satellite validation projects (Aas et al., 2005; Høkedal et al., 2005; Magnusson et al., 2003; Peters et al., 2005a, b; Sørensen et al., 2003, 2004, 2007). The data discussed in this paper were collected during the years 2009–2011, as a part of the ESA-supported VAMP II project.

The advantage of the satellite is that it observes large areas simultaneously, the disadvantage is that the atmosphere influences the recorded radiance, and that the estimates of this influence create some uncertainties. Ship-mounted radiance sensors on ships of opportunity avoid the problem of the atmospheric contribution, but they have to be tilted in order to see a part of the sea surface that is not influenced by the ship. The recorded radiance will then be a function of the reflected sky radiance, the reflected direct radiance from the sun, the water-leaving radiance, the nadir angle of the field-of-view and the azimuth angle relative to the sun, as well as the wind speed. All of these factors constitute a challenge with regard to a quantitative analysis of the recordings (Simis and Olsson, 2013).

Our experience has shown us that a large number of observations under varying conditions are required in order to obtain reliable results. As a first step we have simplified the analysis and the problem by looking at the upward radiance from nadir, and we have investigated the possibility of obtaining the spectral distribution of the water-leaving radiance solely from observations in air. The next step will then be to relate these results to recordings by sensors tilted at an angle from the nadir, so that recordings made by radiometric sensors mounted on ships of opportunity can be used directly for validation of satellite products.

Descriptions of the applied instruments, the series of measurements and the environmental conditions are presented in Sect. 2.1. A way of determining the water-leaving radiance as well as the radiance reflected upwards at the surface from recordings of the sub-surface and above-surface upward nadir radiances is outlined in Sect. 2.2, while a simpler method to estimate the reflected and water-leaving radiances from recordings in air is presented in Sect. 2.3. In Sect. 3.1 the constants necessary for the simple

OSD
12, 1051–1082, 2015

method are calculated, and finally the deviation between the two methods is tested in Sect. 3.2.

2 Material and methods

2.1 Field measurements 2009–2011

In this paper data of the downward spectral irradiance in air, E_{da}, the upward spectral radiance in air from nadir, L_{ua}. and the upward spectral radiance in water from nadir, L_{uw}, will be analysed. These radiometric quantities were recorded by sensors from the TriOS company: E_{da} by the sensor Ramses AAC-VIS (diameter 4.83 cm, length 26 cm), and L_{ua} and L_{uw} by Ramses ARC-VIS (diameter 4.83 cm, length 29.7 cm plus spray protection cap 2.8 cm). Both sensors record by a silicon photodiode array consisting of 256 channels within the range 320–950 nm. The sensors were checked at the start of each field cruise. Data were recorded onboard the R/V *Trygve Braarud* and were stored in a laptop by the MSDA_XE software provided by TriOS. In the post-field processings of the data the wavelengths were restricted to 351 nm and the OLCI (Ocean and Land Colour Instrument) channels up to 754 nm, planned for the Sentinel-3 satellite (ESA): 400, 413, 443, 490, 510, 560, 620, 665, 681, 709 and 754 nm. Except for 351 and 400 nm these correspond to the former MERIS (MEdium Resolution Imaging Spectrometer) channels.

The irradiance sensor was mounted on a pole above the roof of the ship bridge of the R/V *Trygve Braarud*, while the radiance sensor was attached to a rig that measured L_{ua} when the rig was suspended above the sea surface, and L_{uw} when it was submerged in water. The horizontal distance from the rig to the ship side was 3 m. Usually the recording depths in water were 0.5, 1, 1.5, 2, 2.5 and 3 m.

Alltogether 22 series of E_{da}, L_{ua} and L_{uw} have been analysed. The environmental conditions on the four field days are shown in Table 1, and the cloudiness shows that none of the days had a completely clear sky. For each series the ratio (E_{da} (max)-E_{da}

OSD
12, 1051–1082, 2015

(min))/E_{da} (mean) at 560 nm was calculated, and on each day this ratio had a lower and upper value, as displayed by Table 1. We see that the ratio could vary between 0.01 and 1.17, meaning a highly variable downward irradiance. The wind speeds, however, were favourable, being $< 5\,\mathrm{m\,s^{-1}}$. In 2011 the sea showed significant patches of pollen, which do not seem to have influenced the recordings.

At each wavelength in each series of measurement the median of the recorded data was applied, in order to avoid the influence of electronic spikes and other disturbances. However, usually the difference between mean and median values was not significant. In 2009 the variation of E_{da} was greatest (Table 1), and 40 % of the data had relative deviations between median and mean values less than 0.01, 37 % of the data had deviation in the range 0.01–0.05, 16 % had deviations in the range 0.05–0.10, while only 7 % had deviations above 0.10.

The recordings were made in yellow substance-rich coastal waters near the islands of Steilene in the Inner Oslofjord. The bio-optical properties of this area have been presented by Aas et al. (2005), Høkedal et al. (2005) and Sørensen et al. (2003, 2004: 2007). While the annual range of the Secchi disk depth at this location stretches from 2 m during vernal algal bloom to 12 m under winter conditions (Aas et al., 2014), the Secchi disk depths on the four days in Table 1 were in the range 5.0–6.5 m.

Doxaran et al. (2004) made above-surface recordings of the upward radiance from nadir, L_{ua} (0°), and at a tilted angle of 40°, L_{ua} (40°). The azimuth angle relative to the solar plane was 135°. During clear sky conditions the ratio L_{ua} (40°)/L_{ua} (0°) seems to have varied in the ranges 0.9–2.2 and 0.6–2.6 at 450 and 850 nm, respectively. Under an overcast sky the ranges may have been 1.0–1.6 at both wavelengths. This variability may be why we in our first attempt did not obtain satisfactory recordings with radiance sensors at tilted angles.

2.2 Processing of L_{uw} measurements

The radiance from the nadir in water, $L_{uw}(z)$, is a function of the vertical coordinate z, defined positive downwards from the surface. We assume that this function can be

OSD
12, 1051–1082, 2015

approximated by a relationship on the form

$$L_{uw}(z) = L_{uw}(0)\, e^{-K_L z} \tag{1}$$

for monochromatic radiance. K_L is the vertical attenuation coefficient of the radiance, and it is assumed to be practically constant. Due to surface waves it is not possible to measure the radiance value L_{uw} (0) just beneath the surface with sufficient accuracy, but it can be estimated by linear regression analysis of the expression

$$\ln(L_{uw}(z)) = \ln(L_{uw}(0)) - K_L z, \tag{2}$$

where $\ln(L_{uw}(z))$ and z are the variables.

Experience confirms that Eq. (2) describes the vertical attenuation of the radiance $L_{uw}(z)$ fairly well, provided the light conditions in the atmosphere remain constant during the recording. If, on the other hand, the downward irradiance E_{da} in air varies significantly, we have no perfect method to compensate for this. The best way may be to choose a reference value $E_{da,\,ref}$ for the irradiance among those values observed during the recording of $L_{uw}(z)$, and then estimate corrected values of $L_{uw}(z)$ at the different depths by assuming

$$\frac{L_{uw,\,corr}}{E_{da,\,ref}} \approx \frac{L_{uw}(z)}{E_{da}} \tag{3}$$

where E_{da} is the observed irradiance at the time when $L_{uw}(z)$ was recorded.

The recordings of L_{uw} should not be made too close to the ship side. Korsbø and Aas (1997) investigated the influence of ship-shading on upward radiance onboard the R/V *Trygve Braarud* in the Oslofjord. The size of the ship is length 22 m, width 7 m, keel depth 3 m and bridge 6 m above sea surface. Recordings just behind the stern of the ship could typically be reduced by up to 20 %, while recordings at a distance of 5 m did not seem to be influenced by the ship. In the present case the distances have been 3 m, on the sunlit side of the ship, and ship-shading effects have been assumed negligible.

OSD
12, 1051–1082, 2015

While the superstructure of the ship will prevent some of the sky radiance to reach the part of the surface that the radiance sensor is observing, it may also reflect direct solar and diffuse sky radiation towards the same area. This will influence the value of L_w. The problem has been discussed by Hooker and Morel (2003) and Hooker and Zibordi (2005). In our case we think that this reflectance is included in the determination of the ship shading effect.

Another possible source of error is the self-shading effect of downward-looking instruments in the sea. Gordon and Ding (1992) used Monte Carlo simulations to describe this effect, and Zibordi and Ferrari (1995) tested their results by field measurements. Korsbø quantified the self-shading effect in Oslofjorden by in situ measurements (Aas and Korsbø, 1997). The effect was described by

$$\ln(1-\varepsilon) = \ln\left(\frac{L_{\text{uw, meas}}}{L_{\text{uw, true}}}\right) = -BK_L r \quad (4)$$

where ε is the relative error of the measured radiance $L_{\text{uw, meas}}$, and $L_{\text{uw, true}}$ is the true radiance. B is a function of wavelength and solar zenith angel, and Korsbø determined its value by correlation analysis between the variables r and $L_{\text{uw, meas}}$. The radiance sensor has the shape of a cylinder, and r is its radius. From Eq. (4) the correction factor $f(\lambda) = L_{\text{uw, true}}/L_{\text{uw, meas}}$ may be written

$$f(\lambda) = \frac{L_{\text{uw, true}}}{L_{\text{uw, meas}}} = e^{BK_L r} \quad (5)$$

Based on the solar angles in Table 1 and the results of Aas and Korsbø (1997), we have estimated a mean value of B in Eq. (5) equal to $B = (2.5 \pm 0.6)$ for all wavelengths. Combined with the dimensions of the TriOS radiance sensor described in Sect. 2.1, the corresponding value of Br becomes $\text{Br} = (0.09 \pm 0.01)\,\text{m}$. The mean values and standard deviations of K_L and $f(\lambda)$, based on all 22 series of observation for z in the depth range 0.5–3.0 m, are presented in Table 2 at 351 and 400 nm and the MERIS

OSD
12, 1051–1082, 2015

spectral channels in the range 413–754 nm. It illustrates that if the self-shading effect is not taken into account, the extrapolated value of L_{uw} (0) found by Eq. (4) will on average be underestimated by 3–9 % in the Oslofjord by the Ramses-ARC sensor. It should be noted that the small signals produced by the radiance L_{uw} (z) at the smallest and greatest wavelengths increase the uncertainty of the estimated K_L and $f(\lambda)$ at these wavelengths.

When $L_{uw,\,meas}(0)$ has been multplied by the correction factor f, resulting in $L_{uw,\,true}(0)$ according to Eq. (5), the transmittance process through the surface has to be considered. This transmittance is first influenced by Fresnel reflection at the surface, and then by Snell refraction when the radiance enters the air. The first process reduces the radiance by loss of energy flux, and the second process reduces the radiance by spreading the flux into a greater solid angle. The water-leaving radiance L_w is obtained by multiplying $L_{uw,\,true}(0)$ by the conversion factor C_L (Aas et al., 2009):

$$L_w = C_L L_{uw,\,true}(0) \tag{6}$$

Because this value for the water-leaving radiance is based on in-water measurements, we will in later sections denote it as $L_{w,\,meas}$. By inserting for $L_{uw,\,true}(0)$ from Eq. (5), Eq. (6) may then be written

$$L_{w,\,meas} = C_L f(\lambda) L_{uw,\,meas}(0) \tag{7}$$

C_L can be approximated by the value 0.556 according to Morel and Gentili (1996), while Aas et al. (2009) suggested 0.546 for the Oslofjord. The factor can also be determined more precisely by a formula taking into account the wavelength λ, the sea temperature T and the salinity S (Aas et al., 2009). For $T \approx 10\,^\circ$C and $S \approx 20$, the formula becomes:

$$C_L \approx 0.5458 + 0.00003855(\lambda - 550) \tag{8}$$

where λ is in nm.

The radiance sensor was also used in air at a height of 1–2 m above the surface to record the total upward radiance L_{ua} above the same water mass that produced L_w.

OSD
12, 1051–1082, 2015

The radiance meter in air receives light from a greater solid angle than in water, and consequently a different calibration, provided by the TriOS company, has to be applied. The calibration factor F_w for the instrument in water, relative to the calibration factor F_a in air, is (e.g. Aas, 1994)

$$\frac{F_w}{F_a} = \left(\frac{n_g + n_w}{n_g + 1}\right)^2 n_w \tag{9}$$

Here n_g and n_w are refractive indices of the glass window of the radiance meter and the seawater, respectively. They are functions of wavelength, and between 351 and 900 nm the ratio F_w/F_a will vary from 1.774 to 1.722 (Ohde and Siegel, 2003).

2.3 Estimation of reflectance at the surface from L_{ua} and E_{da}

The total upward nadir radiance L_{ua} in air consists of two terms; the Fresnels-reflected upward radiance at the surface L_r and the water-leaving radiance L_w:

$$L_{ua} = L_r + L_w \tag{10}$$

When the water-leaving radiance L_w has been determined from Eq. (7), the upward reflected radiance L_r at the surface can be found from Eq. (10). It was mentioned in the former section that the superstructure of the ship in general may reflect direct solar and diffuse sky radiation towards the field-of-view of the radiance sensor, and thus influence the values of L_r and L_w, but it was also concluded that we think that this effect is negligible in our case.

If there is no wind and the surface is flat, the value of L_r can be estimated from $L_r \approx 0.021 L_{da}$, where L_{da} is the sky radiance from zenith and 0.021 is the value of the Fresnel reflectance for normal incidence at the air–water interface. However, if some wind is present, the estimate of L_r from the zenith radiance can lead to significant errors. Aas (2010) found that the contributions from the sun and the diffuse sky to L_r had to be calculated separately, and polynomials for these calculations were presented.

OSD
12, 1051–1082, 2015

Unfortunately the polynomials require a clear sky, which is not the condition on our field days, as seen by Table 1. Accordingly we need a different method to estimate L_r.

By dividing Eq. (10) by E_{da}, it can be rewritten as

$$R_{ua} = R_r + R_w \tag{11}$$

where $R_{ua}(\lambda)$, $R_r(\lambda)$ and $R_w(\lambda)$ represent the spectral radiance reflectances

$$R_{ua}(\lambda) = \frac{L_{ua}(\lambda)}{E_{da}(\lambda)} \tag{12}$$

$$R_r(\lambda) = \frac{L_r(\lambda)}{E_{da}(\lambda)} \tag{13}$$

$$R_w(\lambda) = \frac{L_w(\lambda)}{E_{da}(\lambda)} \tag{14}$$

R_w is often termed the remote sensing reflectance, as well as the water-leaving reflectance.

By comparing the spectral distributions of $L_r(\lambda)$ and $R_r(\lambda)$ we have noticed that the spectral shape of $R_r(\lambda)$ is more constant than the shape of $L_r(\lambda)$. Consequently we will base our estimation method on an analysis of $R_r(\lambda)$. Figure 1 presents $R_r(\lambda)$ for our series. If we regard R_r (754) as a baseline, and the difference $R_r(351) - R_r(754)$ as a scaling factor, we may be able to describe the spectral shape of $R_r(\lambda) - R_r(754)$ within the interval 351–754 nm by

$$R_r(\lambda) - R_r(754) = A(\lambda)[R_r(351) - R_r(754)] \tag{15}$$

where $A(\lambda)$ is a constant of proportionality. The value of $A(\lambda)$ can be calculated by determining the best-fit line through the origin for $R_r(\lambda)$-R_r (754) as a function of R_r (351)$-R_r$ (754), with the spectral curves of Fig. 1 as input. The results will be presented for the MERIS/OLCI wavelengths in Sect. 3.1.

OSD
12, 1051–1082, 2015

Equation (15) defines $R_r(\lambda)$ as a function of the two variable spectral end-points R_r (351) and R_r (754) and the shape factor $A(\lambda)$. The reflectances R_r (351) and R_r (754) have been obtained from in-water recordings of L_{uw} combined with recordings in air of E_{da}, and accordingly we should search for a method to estimate these reflectances solely from our above-surface recordings. If we transform Eq. (10) to

$$\frac{L_r}{L_{ua}} = 1 - \frac{L_w}{L_{ua}}, \tag{16}$$

this form of the equation gives the useful information that $L_r/L_{ua} \approx 1$ at wavelengths where $L_w/L_{ua} \ll 1$, and we would expect that this was true in the UV and red parts of the spectrum. Ruddick et al. (2006) have pointed out that the spectral shape of $R_w = L_w/E_{da}$ in the near infrared part of the spectrum tends to be constant, because it is dominated by the strong absorption by pure water. This will also influence the spectral shape of R_{ua}. The spectral distribution of $L_r(\lambda)/L_{u,a}(\lambda)$ in our series is presented in Fig. 2.

We see that at 351 and 754 nm the ratio $L_r/L_{ua} = R_r/R_{ua}$ comes much closer to 1 than in the central part of the visible spectrum. If we calculate the best-fit line through the origin for $R_r(351)$ as a function of $R_{ua}(351)$, based on our series, the result may be written

$$R_r(351) \approx C(351)R_{ua}(351) \tag{17}$$

where $C(351)$ is the slope of the line. A similar procedure at 754 nm gives

$$R_r(754) \approx C(754)R_{ua}(754) \tag{18}$$

Figure 3 presents R_r as a function of R_{ua} at 351 and 754 nm. Clearly the deviations from a line through the origine with a slope of 1 are small. By inserting from Eqs. (17) and (18) in Eq. (15), we obtain a relationship for $R_r(\lambda)$ where the only variable input is the values of R_{ua} at 351 and 754 nm:

$$R_r(\lambda) = A(\lambda)C(351)R_{ua}(351) + [1 - A(\lambda)]C(754)R_{ua}(754) \tag{19}$$

OSD
12, 1051–1082, 2015

2.4 Uncertainties of L_{ua}, L_r and L_w

In Sect. 2.1 it was pointed out that the relative differences between our applied median and mean values in 2009 were less than 5 % for 77 % of the data. In the other years with more stable irradiance conditions the deviations are assumed to have been even less.

The calibration of the sensors introduces uncertainties of a similar magnitude. The radiance and irradiance sensors were checked before each field cruise, and they were also regularly calibrated. According to the TriOS company the applied sensors have an "accuracy better than 6 %, depending on spectral range".

Because the water-leaving radiance L_w is obtained from the extrapolated nadir radiance L_{uw} (0) just beneath the surface by Eq. (7), the relative uncertainty $\Delta L_w/L_w$ can be approximated by the similar uncertainty $\Delta L_{uw}(0)/L_{uw}(0)$, where $L_{uw}(0)$ is the radiance extrapolated to the surface by Eq. (2). If we write Eq. (2) as $y = y_0 + K_L z$, where $y = \ln(L_{uw}(z)$ and $y_0 = \ln(L_{uw}(0))$, then the statistical expression for the standard deviation s_{y_0} of y_0 is

$$s_{y_0} = \frac{K_L}{r}\left(\frac{1-r^2}{N-2}\overline{z^2}\right)^{0.5}, r = K_L\frac{s_z}{s_y} \tag{20}$$

where r is the correlation coefficient, N is the number of applied depths, usually 6, and s_y is the standard deviation of y. The average values of $s_{y_0}/y_0 = \Delta L_w/L_w$ are presented in Table 2, and at most of the wavelengths the relative uncertainty is less than 5 %. Based on these estimates, we have assumed that the relative uncertainty of L_{ua} may be around 3 % in the central parts of the studied spectrum, the similar uncertainty of L_w 4 %, and the uncertainty of L_r, depending on L_{ua} as well as L_w, around 5 %. At the border wavelengths 351 and 754 nm the uncertainty of L_w may be greater by a factor of 4–8, as indicated by Table 2.

OSD
12, 1051–1082, 2015

3 Results

3.1 Values of A and C

The spectral values of $A(\lambda)$ in Eq. (15) have been calculated as described in Sect. 2.3, with the spectral curves of Fig. 1 as input. The results are presented for the OLCI wavelengths between 400 and 709 nm in Table 3. Similarly the values of C (351) and C (754) were found by determinations of the best-fit lines for Eqs. (17)–(18), and the results are shown in Table 3.

It is possible to calculate individual values of A and C for each series of measurement. The root-mean-square (rms) deviations between these values and the overall best-fit values of A and C in Table 3, are presented in the last row of Table 3. At 560 nm the deviations constitute more than 50 % of the calculated value of A. Fortunately the accuracy of the estimated radiances is far better than the rms values in Table 3 might suggest. This will be demonstrated in the next section.

3.2 Estimates of R_r, L_r, R_w and L_w

We will denote the estimates of R_r provided by Eqs. (17)–(19) as $R_\mathrm{r,\,est}$. These may then be compared to the values $R_\mathrm{r,\,meas}$ obtained from the field measurements of L_uw, L_ua and E_da. The result is shown by Fig. 4 for the OLCI channels in the range 400–754 nm with the addition of 351 nm. The best-fit line trough the origin obtains the slope 0.984, which is close to 1.

The root-mean-square deviations between $R_\mathrm{r,\,est}$ and $R_\mathrm{r,\,meas}$ are presented for the different wavelengths in Table 4. The rms deviations relative to the mean values are $\leq 13\,\%$. We think this is a satisfactory result when the intention is to use the estimates as a first check of satellite products.

If we multiply Eqs. (17)–(19) by $E_\mathrm{da}(\lambda)$, we obtain the estimates $L_\mathrm{r,\,est}(\lambda)$ at the different wavelengths. These results can be compared to the corresponding measured values $L_\mathrm{r,\,meas}(\lambda)$. Figure 5 presents the estimated vs. the measured reflected radiances.

OSD
12, 1051–1082, 2015

Again the best-fit line obtains a slope close to 1; 1.007. The relative rms deviations for L_r are only slightly greater than the corresponding deviations for R_r, namely $\leq 15\,\%$, as demonstrated by Table 4. At 351 and 754 nm the deviations between estimated and measured values of L_r are only 3 and 1 %, respectively. An important point here is that the estimate of L_r is not obtained from a measured sky radiance multiplied by a Fresnel type of reflection coefficient, depending on the sea roughness, but from the constants A and C and the measured L_{ua} and E_{da}. We assume that this method is valid for solar zenith angles in the range 37–50° and wind speeds up to $5\,\mathrm{m\,s^{-1}}$ in the Oslofjord.

According to Eq. (11) we will obtain the estimate $R_{w,\,est}(\lambda)$ by subtracting $R_{r,\,est}(\lambda)$ from $R_{ua}(\lambda)$. The estimates of this quantity at 351 and 754 nm can be obtained by combining Eqs. (11) and (17)–(18) with the results of Table 3. The results are

$$R_{w,\,est}(351) = (1 - 0.977)R_{ua}(351) = 0.023R_{ua}(351) \tag{21}$$

and

$$R_{w,\,est}(754) = (1 - 0.993)R_{ua}(754) = 0.007R_{ua}(754) \tag{22}$$

The estimated vs. the measured values of R_w at 351 nm and the MERIS/OLCI channels from 400 to 754 nm are shown in Fig. 6. The best-fit line once more obtains a slope close to 1, namely 1.028, but the deviations from the line seem to be greater than in Fig. 5. This, however, is not true. In fact, the rms deviations are exactly the same for $R_{w,\,est}(\lambda)$ as for $R_{r,\,est}(\lambda)$, because Eq. (11) links the two quantities together, and R_{ua} is the same for both the estimated and measured quantities. In Tables 4–5 the rms values are equal for R_r and R_w, but the ratios between the rms and the mean values becomes greater for R_w than for R_r, beacuse the mean values of R_w are much smaller than the corresponding values of R_r.

If we multiply the estimates $R_{w,\,est}(\lambda)$ by $E_{da}(\lambda)$, we obtain the estimates $L_{w,\,est}(\lambda)$, which again can be compared to the measured $L_{w,\,meas}(\lambda)$. Figure 7 presents the estimated vs. the measured water-leaving radiances, and the best-fit line has the slope 0.995. At 560 nm, where the water-leaving radiance has its peak value, the relative rms

OSD
12, 1051–1082, 2015

deviation is 24 % (Table 5), which we think is a surprisingly low value, considering the uncertainties involved. We also consider this rms deviation to be a realistic example of what can be achieved in our waters. Hooker and Zibordi (2005) refer to an accuracy of 5 % required by NASA for ground truth measurements, but this we think can only be achieved under very favourable conditions.

It could be argued that because we have calculated the deviations by the same data set that was applied for the best-fit constants, the test on an independent data set might produce greater deviations. Accordingly we have tried to make such tests by dividing our series into two parts: one for the determination of the constants A and C, and one for the calculation of deviations between measured and estimated reflectances. As an example the 9 series from 2009 have been selected for the determination of A and C, and then these values have been applied to the remaining 13 series from 2010–2011. The results for the radiance reflectance R_r at 560 nm are presented in Table 6. We find that the results for all series together or for the series divided into two parts are not significantly different.

4 Summary and conclusions

We have analysed 22 series of measurement from four field days in the years 2009–2011, collected onboard the R/V *Trygve Braarud* in the Inner Oslofjord. The data consist of recordings of the sub-surface nadir radiance L_{uw}, the corresponding upward radiance L_{ua} in air, and the downward irradiance E_{da} in air. Comments on the data, the applied sensors and the environmental conditions have been presented in Sect. 2.1.

Section 2.2 describes how the water-leaving radiance L_w and the reflected radiance L_r at the sea surface are determined from L_{ua} and L_{uw}. A simpler and much faster method, which determines the reflectance $R_r = L_r/E_{da}$ as well as L_r and L_w solely from the measurements in air of L_{ua} and E_{da}, is presented in Sect. 2.3. The coefficients A and C, defined by Eqs. (15) and (17)–(18), are key parts of this method, and they are

OSD
12, 1051–1082, 2015

quantified in Sect. 3.1. The applied wavelengths are 351 nm in addition to the 11 OLCI channels in the range 400–754 nm.

A comparison between the quantities determined by the two methods shows that the average relative deviations between their results are less than or equal to 13 and 15 % for R_r and L_r, respectively (Sect. 3.2). The deviations of the water-leaving radiance L_w and the corresponding reflectance $R_w = L_w/E_{da}$ are identical to those of R_r and L_r when measured in absolute units, but in relative units they become greater, because R_w and L_w are smaller than R_r and L_r. On the other hand, at 560 nm where L_w obtains its maximum values, the average relative deviation between the two methods is still only 24 % for both R_w and L_w, and we consider this to be an acceptable uncertainty of the estimates.

Our overall conclusion is that the suggested method to estimate reflected and water-leaving radiances, based on measurements in air of upward nadir spectral radiance and downward spectral irradiance, provides results with a satisfactory accuracy. The remaining task is to determine the relationships between radiance from nadir and radiance recorded by tilted sensors. The recordings made by radiometric sensors mounted on ships of opportunity can then be used for validation of the remote sensing reflectance estimated by satellites, at significantly lower costs than those required by the use of research vessels.

Author contributions. All authors participated in parts of the field work. Post-field processing of the data were made by A. Folkestad and Ø Kleiv. K. Sørensen directed the project. E. Aas prepared the manuscript with comments and data from the co-authors.

Acknowledgements. The field work and the first processing of the data was part of the PRODEX project C90383 “Validation of MERIS products – VAMP II”, supported by ESA. A minor part of the data processing was supported by the Department of Geosciences at the University of Oslo.

OSD
12, 1051–1082, 2015

References

Aas, E.: A simple method for radiance calibration, in: European Workshop on Optical Ground Truth Instrumentation for the Validation of Space-Borne Optical Remote Sensing Data of the Marine Environment, 23–25 November 1993, Netherlands Institute for Sea Research, Texel, the Netherlands, Rep. 1994-3, 39–44, 1994.

Aas, E.: Estimates of radiance reflected towards the zenith at the surface of the sea, Ocean Sci., 6, 861–876, doi:10.5194/os-6-861-2010, 2010.

Aas, E. and Korsbø, B.: Self-shading effect by radiance meters on upward radiance observed in coastal waters, Limnol. Oceanogr., 42, 968–974, 1997.

Aas, E., Høkedal, J., and Sørensen, K.: Spectral backscattering coefficient in coastal waters, Int. J. Remote Sens., 26, 331–343, 2005.

Aas, E., Høkedal, J., and Højerslev, N. K.: Conversion of sub-surface reflectances to above-surface MERIS reflectance, Int. J. Remote Sens., 30, 5767–5791, 2009.

Aas, E., Høkedal, J., and Sørensen, K.: Secchi depth in the Oslofjord–Skagerrak area: theory, experiments and relationships to other quantities, Ocean Sci., 10, 177–199, doi:10.5194/os-10-177-2014, 2014.

Doxaran, D., Nagur Cherukuru, R. C., and Lavender, S. J.: Estimation of surface reflection effects on upwelling radiance field measurements in turbid waters, J. Opt. A-Pure Appl. Op., 6, 690–697, 2004.

Gordon, H. R. and Ding, K.: Self-shading of in-water optical instruments, Limnol. Oceanogr., 37, 491–500, 1992.

Hooker, S. B. and Morel, A.: Platform and environmental effects on above-water determinations of water-leaving radiances, J. Atmos. Ocean. Tech., 20, 187–205, 2003.

Hooker, S. B. and Zibordi, G.: Platform perturbations in above-water radiometry, Appl. Optics, 44, 553–567, 2005.

Høkedal, J., Aas, E., and Sørensen, K.: Spectral optical and bio-optical relationships in the Oslo Fjord compared with similar results from the Baltic Sea, Int. J. Remote Sens., 26, 371–386, 2005.

Korsbø, B. and Aas, E.: Ship-shading effects on upward radiance and irradiance in coastal waters, Rep. Dept. Geophys., Univ. Oslo, Oslo, Norway, 101, 13 pp., 1997.

Kristiansen, T. and Aas, E.: Water type quantification in the Skagerrak, the Kattegat and off the Jutland west coast, Oceanologia, 57, 177–195, 2015.

OSD
12, 1051–1082, 2015

Estimation of upward radiances and reflectances

Ø. Kleiv et al.

Magnusson, J., Dahl, E., Karud, J., Sørensen, K., Willbergh, M., and Aas, E.: Validation of methods for monitoring of coastal and open sea areas with satellites and sensors on ships of opportunity, NIVA Report SNO 4710-2003, NIVA, Oslo, Norway, 2003.

Morel, A. and Gentili, B.: Diffuse reflection of oceanic waters. II. Bidirectional aspects, Appl. Optics, 35, 4850–4862, 1996.

Ohde, T. and Siegel, H.: Derivation of immersion factors for the hyperspectral TriOS radiance sensor, J. Opt. A-Pure Appl. Op., 5, L12–L14, doi:10.1088/1464-4258/5/3/103, 2003.

Peters, S. W. M., Eleveld, M., Pasterkamp, R., van der Woerd, H., Devolder, M., Jans, S., Park, Y., Ruddick, K., Block, T., Brockmann, C., Doerffer, R., Kraseman, H., Röttgers, R., Schönfeld, W., Jørgensen, P. V., Tilstone, G., Martinez-Vincente, V., Moore, G., Sørensen, K., Høkedal, J., Johnsen, T. M., Lømsland, E. R., and Aas, E.: Atlas of Chlorophyll-a concentration for the North Sea based on MERIS imagery of 2003, Vrije Universiteit, Amsterdam, the Netherlands, 121 pp., 2005a.

Peters, S., Brockmann, C., Eleveld, M., Pasterkamp, R., van der Woerd, H., Ruddick, K., Park, Y., Block, T., Doerffer, R., Krasemann, H., Roettgers, R., Schoenfeld, W., Joergensen, P., Tilstone, G., Martinez-Vicente, V., Moore, G., Soerensen, K., Hokedal, J., and Aas, E.: Regional chlorophyll retrieval algorithms for North Sea waters: intercomparison and validation. Proceedings of the MERIS (A)ATSR Workshop 2005 (ESA SP-597). 26–30 September 2005 ESRIN, Frascati, Italy, Edited by: Lacoste, H., Published on CDROM, p.19.1 Publication Date: 12/2005, 2005b.

Ruddick, K. G., De Cauwer, V., and Park, Y.: Seaborne measurements of near infrared water-leaving reflectance: the similarity spectrum for turbid waters, Limnol. Oceanogr., 51, 1167–1179, 2006.

Simis, S. G. H. and Olsson, J.: Unattended processing of shipborne hyperspectral reflectance measurements, Remote Sens. Environ., 135, 202–212, 2013.

Sørensen, K., Høkedal, J., Aas, E., Doerffer, R., and Dahl, E.: Early results for validation of MERIS water products in the Skagerrak. Proceedings of “Envisat Validation Workshop”, 9–13 December 2002, Frascati, Italy (ESA SP-531, March 2003), 2003.

Sørensen, K., Aas, E., Høkedal, J., Severinsen, G., Doerffer, R., and Dahl, E.: Validation of MERIS water products in the Skagerrak. MAVT Workshop. Proceedings of Envisat Validation Workshop, 20–24 October 2003, Frascati, Italy (ESA CD-ROM), 2004.

Sørensen, K., Aas, E., and Høkedal, J.: Validation of MERIS water products and bio-optical relationships in the Skagerrak, Int. J. Remote Sens., 28, 555–568, 2007.

OSD
12, 1051–1082, 2015

Zibordi, G. and Ferrari, G. M.: Instrument self-shading in underwater optical measurements: experimental data, Appl. Optics, 34, 2750–2754, 1995.

OSD
12, 1051–1082, 2015

OSD
12, 1051–1082, 2015

Table 1. Environmental conditions during field work at 59°49′ N 10°34′ E.

Date	Wind speed [$\mathrm{m\,s^{-1}}$]	Cloudiness [octas]	Mean cloudiness [octas]	Solar zenith angle [°]	Number of series	Range/mean of E_{da} at 560 nm
25 June 2009	2.8	1–3	1.7	37–50	9	0.01–1.17
6 May 2010	2.5	4–8	6.3	43–44	3	0.09–0.43
7 May 2010	4.9	2–3	2.3	43–51	7	0.01–0.36
10 May 2011	2.3	4–6	5.3	45–50	3	0.02–0.33

Table 2. Mean value ± standard deviation of the vertical attenuation coefficient K_L of sub-surface radiance from nadir, of the correction factor f for self-shading by the radiance sensor, and of the relative uncertainty $\Delta L_w/L_w$ of the water-leaving radiance at different wavelengths λ. The number of analysed series is 22.

λ [nm]	K_L [m^{-1}]	f	$\Delta L_w/L_w$
351	1.08 ± 0.17	1.102 ± 0.017	0.277 ± 0.139
400	1.01 ± 0.12	1.095 ± 0.012	0.077 ± 0.034
413	0.99 ± 0.14	1.093 ± 0.014	0.052 ± 0.033
443	0.73 ± 0.10	1.068 ± 0.010	0.045 ± 0.034
490	0.45 ± 0.08	1.042 ± 0.007	0.039 ± 0.036
510	0.39 ± 0.07	1.036 ± 0.007	0.038 ± 0.038
560	0.29 ± 0.05	1.026 ± 0.005	0.037 ± 0.046
620	0.44 ± 0.05	1.041 ± 0.005	0.042 ± 0.044
665	0.53 ± 0.05	1.049 ± 0.005	0.043 ± 0.042
681	0.47 ± 0.05	1.043 ± 0.005	0.047 ± 0.046
709	0.69 ± 0.06	1.064 ± 0.006	0.063 ± 0.041
754	0.50 ± 0.11	1.046 ± 0.010	0.158 ± 0.073

OSD
12, 1051–1082, 2015

Table 3. Best-fit values of A in the range 400–709 nm, and of C at 351 and 754 nm, and the rms deviations between these values and individual calculations of A and C at the wavelengths λ.

λ [nm]	A or C	rms
351	0.977	0.039
400	0.661	0.047
413	0.567	0.060
443	0.470	0.078
490	0.444	0.139
510	0.433	0.156
560	0.429	0.248
620	0.198	0.095
665	0.129	0.061
681	0.147	0.079
709	0.078	0.039
754	0.993	0.031

OSD
12, 1051–1082, 2015

Table 4. Mean values of measured radiance reflectance $R_{r,\,meas}$ and reflected radiance $L_{r,\,meas}$, and the rms deviations between these quantities and the corresponding estimated values.

λ	$R_{r,\,meas}$			$L_{r,\,meas}$		
	mean	rms	$\frac{rms}{mean}$	mean	rms	$\frac{rms}{mean}$
[nm]	[$10^{-5}\,sr^{-1}$]		[%]	[$10^{-2}\,mW\,m^{-2}\,nm^{-1}\,sr^{-1}$]		[%]
351	615	17	2	157	4.5	3
400	477	21	4	229	10	4
413	438	25	6	249	13	5
443	400	23	6	264	16	6
490	393	29	7	276	24	9
510	389	32	8	277	27	10
560	391	50	13	274	42	15
620	289	27	9	172	18	10
665	260	22	9	144	14	9
681	268	27	10	144	16	11
709	237	20	8	117	11	9
754	205	2.1	1	88	1.3	1

OSD
12, 1051–1082, 2015

Table 5. Mean values of measured remote sensing reflectance $R_{\text{w, meas}}$ and water-leaving radiance $L_{\text{w, meas}}$, and the rms deviations between these quantities and the corresponding estimated values.

λ	$R_{\text{w, meas}}$			$L_{\text{w, meas}}$		
	mean	rms	$\frac{\text{rms}}{\text{mean}}$	mean	rms	$\frac{\text{rms}}{\text{mean}}$
[nm]	[10^{-5} sr^{-1}]		[%]	[10^{-2} mW m^{-2} nm^{-1} sr^{-1}]		[%]
351	19	17	89	5.2	4.5	87
400	71	21	29	39	10	25
413	74	25	33	48	13	28
443	97	23	24	74	16	21
490	146	29	20	120	24	20
510	164	32	19	137	27	20
560	213	50	24	173	42	24
620	95	27	28	71	18	25
665	62	22	36	45	14	30
681	67	27	40	46	16	35
709	32	20	63	21	11	52
754	2.9	2.1	72	1.6	1.3	80

OSD
12, 1051–1082, 2015

OSD
12, 1051–1082, 2015

Estimation of upward radiances and reflectances

Ø. Kleiv et al.

Table 6. Values of A and C and the measured radiance reflectance $R_{\mathrm{r,\,meas}}$ at 560 nm for all series taken together, and for the test case with A and C determined from 9 series and applied on the remaining 13 series. The rms represents the deviations between $R_{\mathrm{r,\,meas}}$ and the corresponding estimated values of $R_{\mathrm{r,\,est}}$.

Number of series	C (351)	A (560)	C (754)	$R_{\mathrm{r,\,meas}}$ (560) mean [10^{-5} sr^{-1}]	rms	$\frac{\mathrm{rms}}{\mathrm{mean}}$ [%]
22	0.977	0.429	0.993	391	50	13
9 selected	0.955	0.488	0.990	390	63	16
13 extra				392	48	12

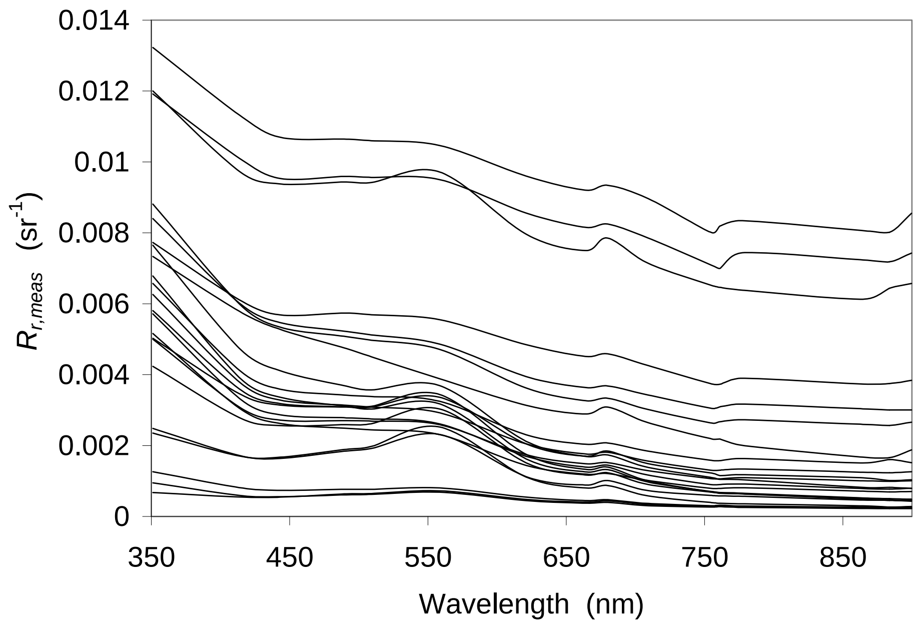

Figure 1. Spectral distribution of the measured radiance reflectance $R_{\text{r, meas}}$.

OSD
12, 1051–1082, 2015

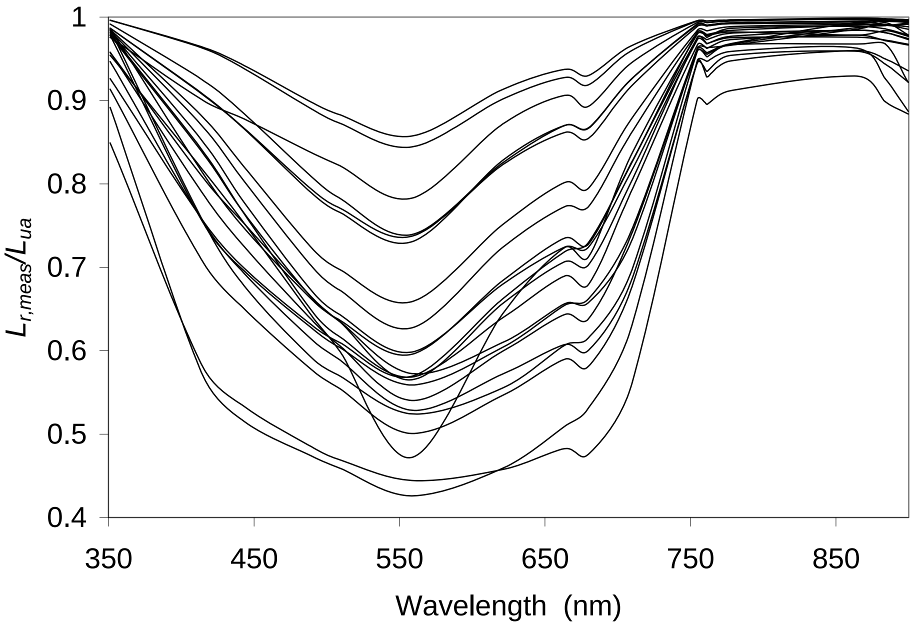

Figure 2. Spectral distribution of the ratio $L_{\mathrm{r,\,meas}}/L_{\mathrm{ua}}$.

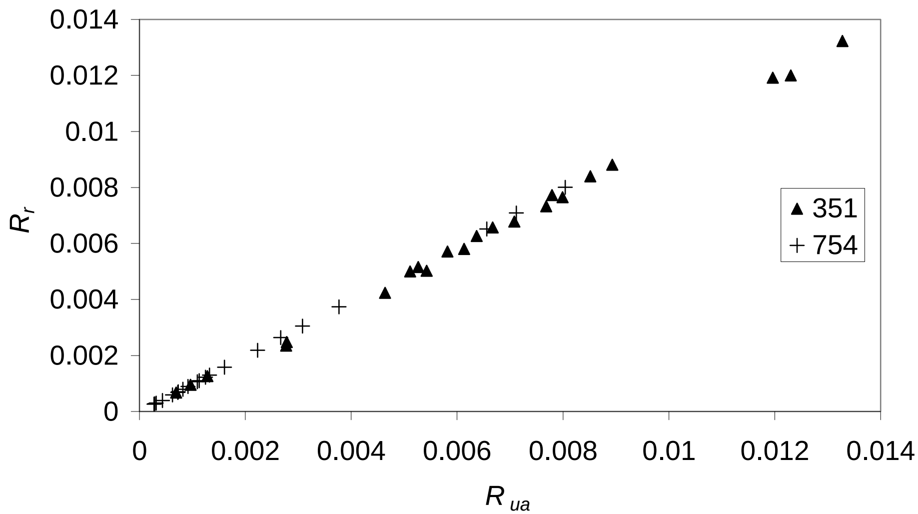

Figure 3. The upward radiance reflectance in air, R_r, as a function of the total upward reflectance in air, R_{ua}, at 351 and 754 nm.

OSD
12, 1051–1082, 2015

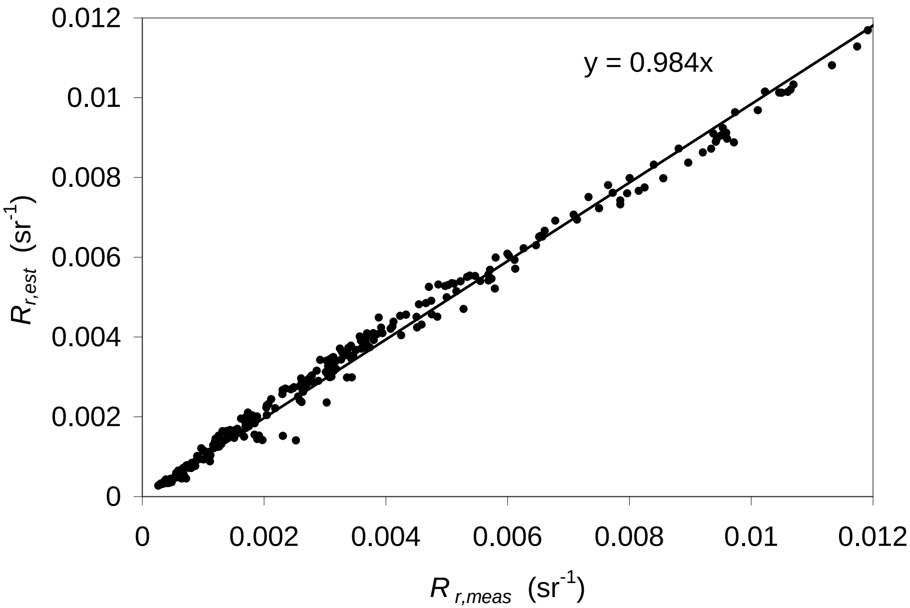

Figure 4. Estimated vs. measured values of the radiance reflectance R_r for all series and wavelengths.

OSD
12, 1051–1082, 2015

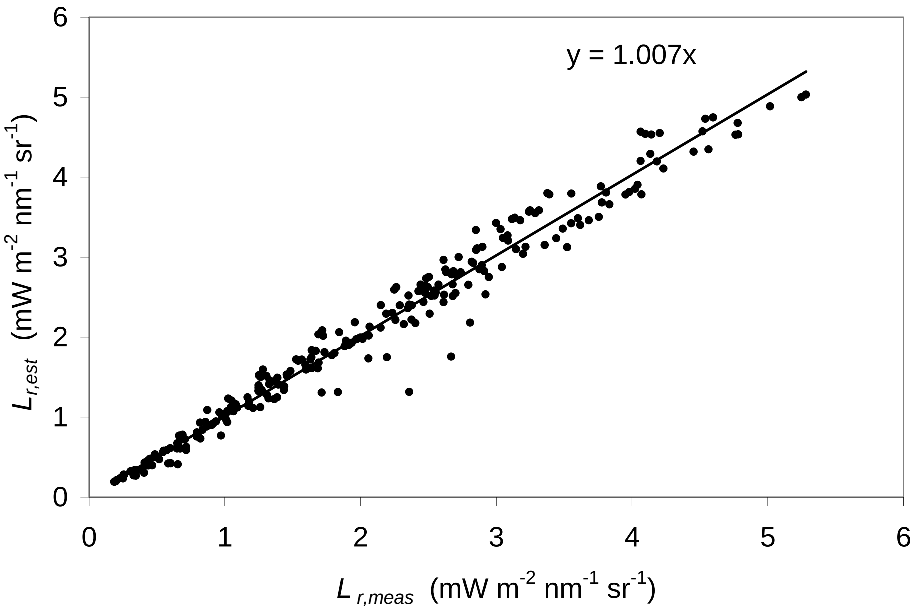

Figure 5. Estimated vs. measured values of the reflected radiance L_r for all series and wavelengths.

OSD
12, 1051–1082, 2015

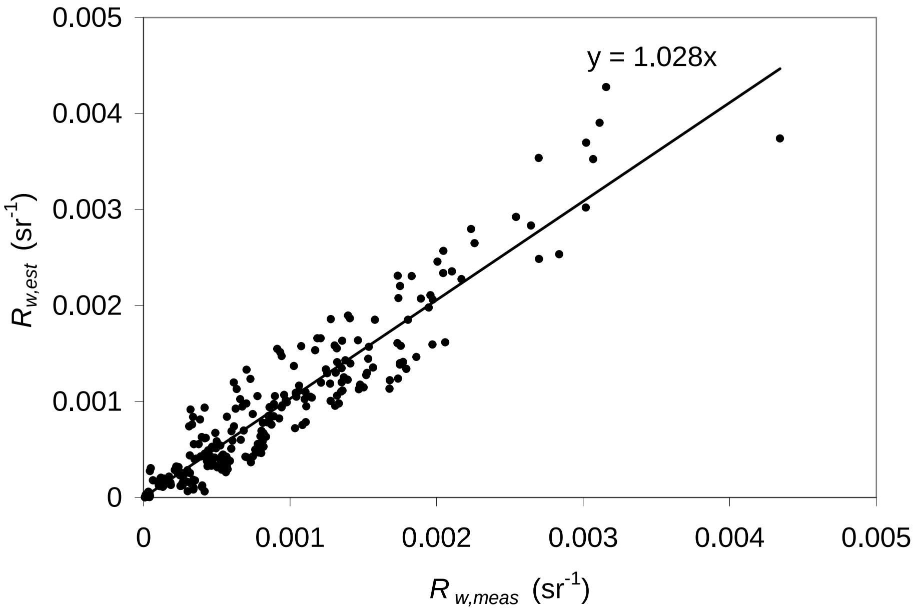

Figure 6. Estimated vs. measured values of the remote sensing reflectance R_w for all series and wavelengths.

OSD
12, 1051–1082, 2015

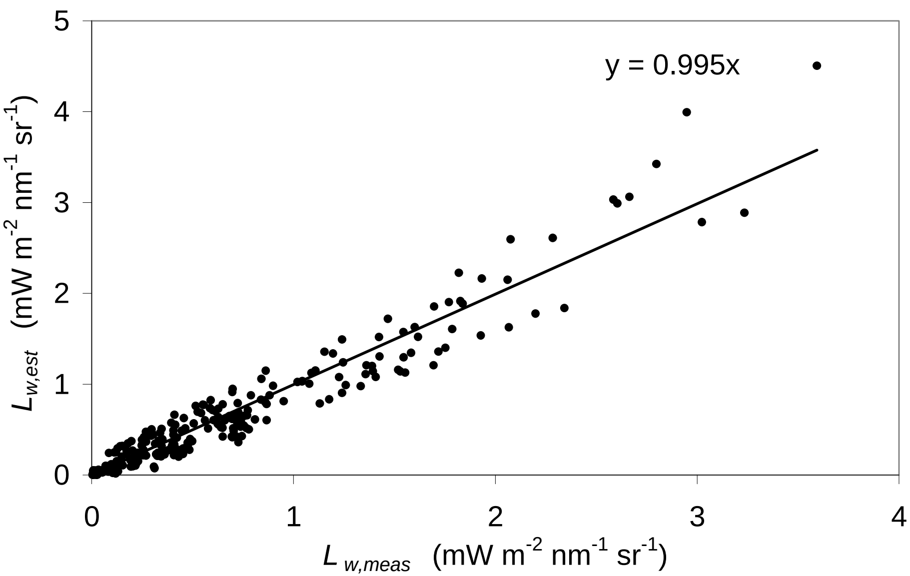

Figure 7. Estimated vs. measured values of the water-leaving radiance L_w for all series and wavelengths.